Proposal

Intermediate Silicon Tracker for the STAR Tracking Upgrade

January 2007

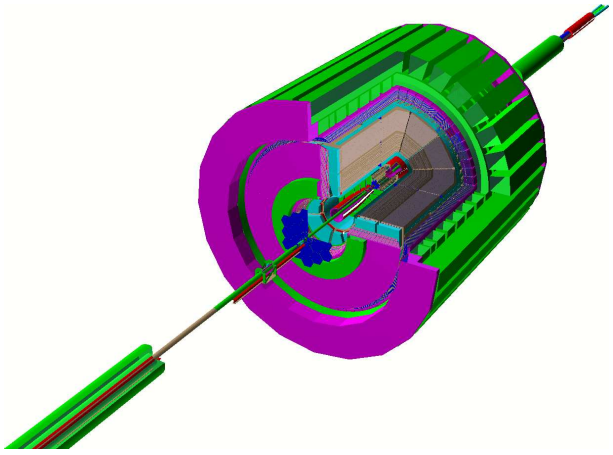

Proposal

Integrated Tracking Upgrade for the STAR experiment

H. Spinka, D. Underwood
Argonne National Laboratory, Argonne, IL, USA

D. Beavis, R. Debbe, J.H. Lee, F. Videbaek
Brookhaven National Laboratory, Upton, NY, USA

H.S. Matis, H.G. Ritter, A. Rose, E. Sichtermann, J.H. Thomas, W. Wieman, N. Xu
Lawrence Berkeley National Laboratory, Berkeley, CA, USA

D. Hasell, J. Kelsey, M. Miller, R. Milner, M. Plesko, R. Redwine, D. Ross, F. Simon, B. Surrow, G. van Nieuwenhuizen
Massachusetts Institute of Technology, Cambridge, MA, USA

Contents

1 Executive Summary

The STAR collaboration is preparing a challenging tracking detector upgrade program to further investigate fundamental properties of the new state of strongly interacting matter produced in relativistic-heavy ion collisions at RHIC and to provide fundamental studies of the nucleon spin structure and dynamics in high-energy polarized proton-proton collisions at RHIC.

A key step in this direction is the ability for the direct reconstruction of charm and beauty decays as well as flavor tagged jets to allow a precise measurement of the spectra, yields and flow of open charm and beauty production. The measurement of the nuclear modification factor R_{AA} from central to peripheral collisions is a critical step for particles containing heavy quarks. This will allow fundamental tests of QCD predictions of heavy quark energy loss. The measurement of heavy quark (charm/beauty) production in polarized proton-proton collisions would allow an extension of the capabilities to measure the gluon contribution to the proton spin in particular towards lower values of the gluon momentum fraction [1]. The measurement of heavy quark production in gluon-gluon initiated processes, $gg \rightarrow Q\bar{Q}$, would provide a stringent test of the underlying Standard Model dynamics for both unpolarized and polarized measurements [2].

The reconstruction of open charm and beauty production requires a precision micro-vertex detector and intermediate tracking detector capable of directly observing charm and beauty decays. This is the focus of the Heavy Flavor Tracker (HFT), a high-resolution micro-vertex detector based on active pixel sensor (APS) technology in combination with a new Intermediate Silicon Tracker (IST). The reconstruction of open charm and beauty production in proton-proton collisions and for low multiplicity events in relativistic heavy-ion collisions in particular, requires a new intermediate tracking system together with the existing STAR silicon-strip detector (SSD) and the STAR Time-Projection Chamber (TPC). This new silicon barrel detector, the Intermediate-Silicon Tracker (IST), is expected to replace the current STAR Silicon Vertex Tracker (SVT) which is based on silicon drift detectors. The IST would establish a track-pointing device for the HFT, connecting TPC tracks to the high-precision inner HFT layers. The design is chosen in such a way to provide independent tracking capabilities based on the IST for beauty production at a center-of-mass energy of 500 GeV in polarized proton-proton collisions. The anticipated design of the IST will be compatible with the STAR Data Acquisition Upgrade (DAQ1000). A combination

of well-established silicon strip sensors and silicon pad sensors is foreseen for the IST design.

It should be stressed that the integrated tracking upgrade for STAR based on well-established, intrinsically fast detector and readout elements, will provide a significant improvement of the existing STAR tracking system, in particular for the expected high luminosity operation at RHIC. The proposed design will allow to have tracking information available at the trigger level. This will aid the selection of rare events already at the trigger level.

The following document provides a detailed account of the physics motivation (Section 2) of the integrated tracking upgrade project for heavy flavor production in relativistic-heavy ion collisions. A conceptual layout (Section 3) within the detector simulation package GEANT and a first conceptual engineering design based on Solidworks has been completed. The anticipated detector technology (Section 4) is based on well-established tracking technology such as silicon strip and silicon pad sensors. The readout system for the intermediate tracking system are based on the APV25-S1 readout chip which has been extensively tested for the CMS silicon tracker and is also used by the COMPASS triple-GEM tracking stations.

2 Physics motivation

2.1 Relativistic Heavy-Ion program

With the advent of the Relativistic Heavy Ion Collider (RHIC) high energy nuclear physics has made a giant leap forward. RHIC and its four experiments were constructed to study matter at the highest matter- and energy-densities possible in the laboratory. This is being achieved by colliding gold nuclei at a maximum center of mass energy of 200 GeV per nucleon and detecting the particles coming out of the collision with high precision detectors. The goal is to recreate matter in a state as it existed only a few micro-seconds after the Big Bang.

The RHIC heavy ion program has been immensely successful. Not only did the collider exceeded it's expected performance, also the experiments were able to keep up with the enormous amount of data that accumulated in only a few years time. The general outcome of the different physics analysis was striking [3]. The common belief before the startup of RHIC was that it would create a state of matter where quarks and gluons would be asymptotically free [4], the so called Quark Gluon Plasma (QGP). In this gaseous state color would be deconfined and chiral symmetry restored. After comparing most of the results the experiments have now come to the conclusion that not a gaseous state has been created but rather an almost perfect liquid state where the constituents are stronly interacting. The discovery of this strongly interacting QGP will have interesting implications for Big Bang theories and possibly also for the description of the structure of the universe as it is being observed right now.

The conclusion that a strongly interacting system with a high energy density is formed is based on several observations. These observations are discussed in the following sections.

2.1.1 Characterizing the medium

Figure 1 shows the charge particle densities around mid-rapidity for heavy ion collisions from AGS, through SPS to RHIC energies. The charged particle densities at top RHIC energy are about twice those obtained at the maximum SPS energies. The transverse energy per particle doesn't seem to have decreased by going from SPS to RHIC energies. Therefor, the energy density at top RHIC energy can be expected to be, at least, twice as high as

was obtained at the maximum SPS energy.

A more rigorous value for the energy density can be calculated by combining the measured charged particle densities with estimates for the mean energy per particle and the expected system size. Since there is now transverse momenta data available for identified charged particles from about 30 MeV/c to several GeV/c, it is possible to obtain a reasonable value for the average transverse momenta (500 MeV/c). This, together with some assumptions (for instance the number of not detected neutral particles), leads to a total energy of all emitted particles around mid-rapidity of 1600 GeV. The system volume is, for central Au+Au collisions, determined by the transverse area of the Au nuclei (150fm^2) and the longitudinal size. The last is roughly determined by the time that it takes for the system to equilibrate. According to the elliptic flow results this should be about $1 - 2\text{fm/c}$. So, the energy density of the equilibrated system is expected to be > 3 GeV/fm^3. This is well beyond the energy density where the transition from a hadronic to a deconfined system is believed to take place [5].

Until now almost all information has been obtained by observing particles consisting out of the light quarks (u,d,s). Since light quark production takes place during the whole course of the collision, the information from the early stages of the collision is largely washed out. The heavier quarks (c,b), due to their large mass, are predominately being produced during the initial hard scattering stage of the collision. Charm can also be produced by gluon fusion during the pre-equilibrium stage and, provided that the temperature is above 500 MeV, thermal charm production becomes a possibility. Due to its much larger mass beauty is only produced by hard scattering. Therefor, being able to identify charmed and beauty hadrons will give an important new handle on the dynamics of the collision. The relative yields of charm and beauty and more specifically charm enhancement due to thermal production will yield valuable information about the energy density of the created system.

2.1.2 Transverse momentum spectra

In the initial stage of the collision hard scattered partons will lead to jet production, i.e. a collimated stream of high momentum particles will emerge at mid-rapidity. In p+p and e+p collisions these jets, usually back-to-back, are easy to distinguish. In heavy ion collisions not only are there multiple jets per collision but also other processes lead to such an abundance of particles that jets can not be distinguished individually anymore. However, particles

in the jets are very energetic and so, in an indirect way, jet production can be studied by looking for high transverse momentum particles.

Well before the advent of RHIC it was predicted that the hard scattered partons would be 'slowed down' by the hot and dense matter created in a heavy ion collision[6, 7, 8]. This would lead to less energy being available for the jets and to an apparent suppression of high transverse momentum particles relative to p+p collisions. This effect was indeed observed and is illustrated in figure2. The nuclear modification factor R_{AA} is defined as:

$$R_{AA} = \frac{\sigma_{pp}^{inel}}{< N_{coll} >} \frac{d^2 N_{AA}/dp_T d\eta}{d^2\sigma_{pp}/dp_T d\eta} \quad (1)$$

So, basically, the p_T spectra of the heavy ion collision divided by the p_T spectra of the p+p collision, properly scaled by the inelastic nucleon-nucleon cross section and the number of expected binary nucleon-nucleon collisions in the heavy ion collision.

Unfortunately the observed heavy ion spectra are a convolution of hard and soft processes and only give a time average over the whole course of the collision. Final state particles containing light quarks (up, down and strange) can be coming from all stages of the collisions and so effects like high p_T suppression are largely washed out. Heavier quarks (charm and beauty) are presumed to be created mainly in the initial hard scattering phase of the collision. Therefor, observing particles carrying heavy flavor should provide information about the energy loss of the heavier quarks in the created medium. It must be stated that the expected smaller energy loss of heavier quarks ('dead cone' effect [9]) could complicate matters a bit.

Like with the existing measurements of the nuclear modification factor it will also for the new heavy quark measurements be important to have measurements for a wide range of centralities. To set proper baselines it will be again necessary to observe charm and beauty production for different collision systems, especially d+A comes to mind.

2.1.3 Flow

Elliptic flow originates from the geometrical overlap region in the first stages of the collision. In a strongly interacting medium the frequent interactions lead to a collectivity which is being observed as a strong flow signal in the final state. As the system expands the information about the initial state gets lost and the elliptic flow saturates.

By studying the elliptic flow as a function of p_T and using hydrodynamical models it was found out that the observed elliptic flow gets 'generated' in the very early stages of the collision, setting a constraint on the time needed for thermalization, see figure 3. This conclusion was reached by detecting final state particles mainly consisting out of light quarks which are interacting strongly with the surrounding hot medium, even after most of the initial geometrical information has been washed out.

Heavy quarks couple much weaker to the medium and performing the same measurements with heavy quark hadrons would, hopefully, yield a much cleaner signal of the thermalization time than the existing light flavor observations.

Since the elliptic flow is strongly dependent on the centrality of the collision, the measurements with heavy flavor hadrons should be done over a large centrality range.

2.2 Heavy flavor physics

Heavy-quark (charm, beauty) production is a versatile environment for quantitative tests of quantum chromodynamics (QCD) and the interplay of perturbative and non-perturbative phenomena. Their measurement is attractive at RHIC since the production cross section is large, $\mathcal{O}(10^2 - 10^3)\mu$b and the dominant production mechanism is gluon-gluon fusion: a gluon from one proton coupling a gluon from the other proton by forming a quark anti-quark pair. A quantitative description of the process requires the knowledge of the gluon momentum distribution in the proton, the calculation of the hard gluon gluon subprocess, and fragmentation functions which account for the long-range effects binding the heavy quark in a hadron.

Since the heavy quark mass sets a large scale, calculations can be performed for small transverse momenta or even for total cross sections. This is in distinct contrast to the production of particles composed solely of light quarks, where one relies on large transverse momenta to overcome the presently incalculable complication of soft processes. Assuming the applicability of perturbative QCD will be demonstrated in the RHIC environment, e.g. by the comparison of the cross sections from experiment and theory, measurements involving heavy quark production should give access to the gluon density at smaller x-values than measurements for jet or prompt-photon production at similar pseudo-rapidities and (necessarily) larger scale.

Significant progress, experimentally and theoretically, has been made in

the long-standing discrepancy between bottom production rates at the TeVatron and NLO QCD theory; calculations are in reasonable agreement with data. Charm measurements at $\sqrt{s} = 1.96\,\mathrm{TeV}$ exist for high transverse momenta only, where the central values for the cross section appear higher than NLO predictions by ∼50%. The apparent difference is, however, covered by substantial experimental and theoretical uncertainties. Complete next-to-leading order QCD corrections to the *polarized* hadroproduction of heavy flavors have recently been completed.

At RHIC the decay of heavy-flavor mesons forms the dominant contribution in the inclusive production of leptons at intermediate to large transverse momenta ($\sim 2 < p_T <\sim 10\,\mathrm{GeV}$). First measurements of the unpolarized cross-section for inclusive electrons have been reported. Polarized measurements of inclusive electron production should become within reach while RHIC develops to achieve its integrated luminosities of 320 at $\sqrt{s} = 200\,\mathrm{GeV}$ and 800 at $\sqrt{s} = 500\,\mathrm{GeV}$ projected for the spin physics program.

Experimental challenges are many, and of course include clean identification. Rejection of the sizable backgrounds, in particular those from pion Dalitz decays and photon conversion, is of particular importance. To discriminate signal from background sources, two (potential) observables have been widely used; they are based on the large mass and on the relatively long lifetime.

The high mass gives rise to aforementioned large values of the transverse momenta of the decay lepton (electron). With the completion of the EM-calorimeters, STAR has trigger capability for electrons/positrons and meaningful initial measurements of e.g. inclusive electron asymmetries can thus be made with integrated luminosities of $10\,\mathrm{pb}^{-1}$ or more.

The remarkable achievements on the charm structure function F_2^c at HERA, the photon structure function F_2^γ at LEP, and the heavy quark measurements at the TeVatron demonstrate the need to exploit the second observable in the production of heavy quarks, the lifetime. The lifetime of heavy D and B mesons can be exploited as a "tag" by observing the tracks from secondary charm and beauty vertices. In these measurements precision tracking allows the selection of jets containing hadrons with heavy quarks via the identification of secondary vertices, and of jets originating from a secondary vertex. STAR is uniquely suited for jet measurements at RHIC. However, STAR does *not* currently have a high-rate precise tracking capability. Its development and implementation form the thrust of the present proposal.

Realistic projections for the potential sensitivities require simulation that involve detailed jet algorithm studies and a realistic detector description. At this time studies of this nature are being developed using the conceptual layout outlined in chapter 4. Sensitivity of the *baseline* measurement of inclusive electrons is illustrated in Fig. 4. It accounts for realistic branching ratios, trigger capability with EM-calorimeter towers, STAR acceptance, and sampling of the beam diamond with future high-precision inner trackers.

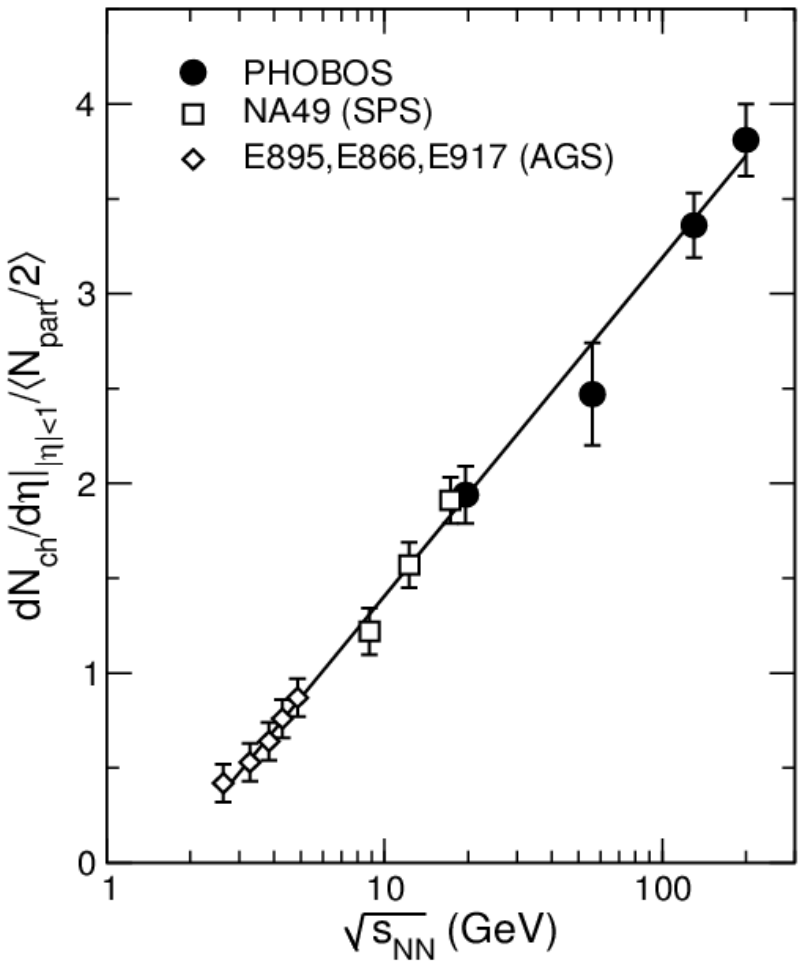

Figure 1: *The pseudo-rapidity charged particle densities at mid rapidity as a function of collision energy.*

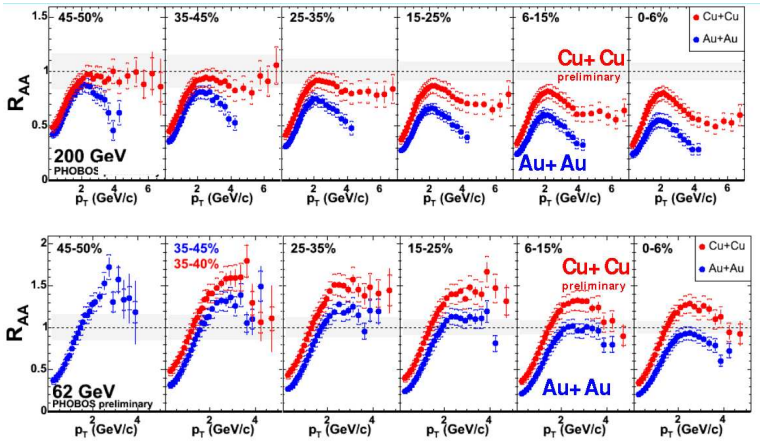

Figure 2: R_{AA} *versus* p_T *for Au+Au and Cu+Cu at 200 (top) and 63 GeV (bottom).*

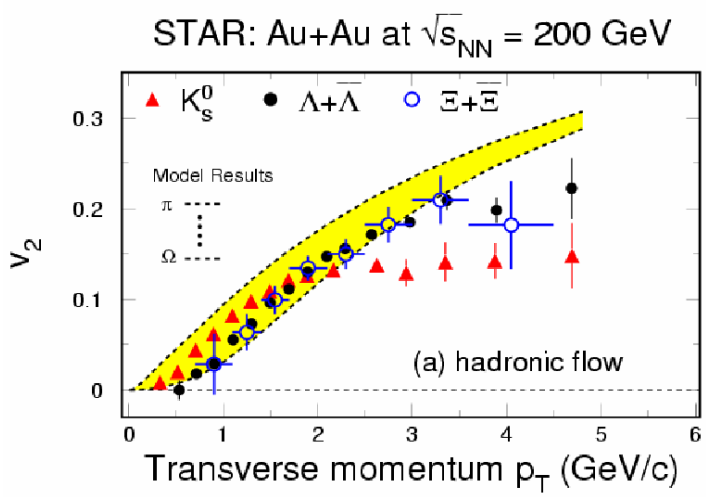

Figure 3: *Elliptic flow of strange hadrons versus* p_T *for Au+Au at 200 GeV.*

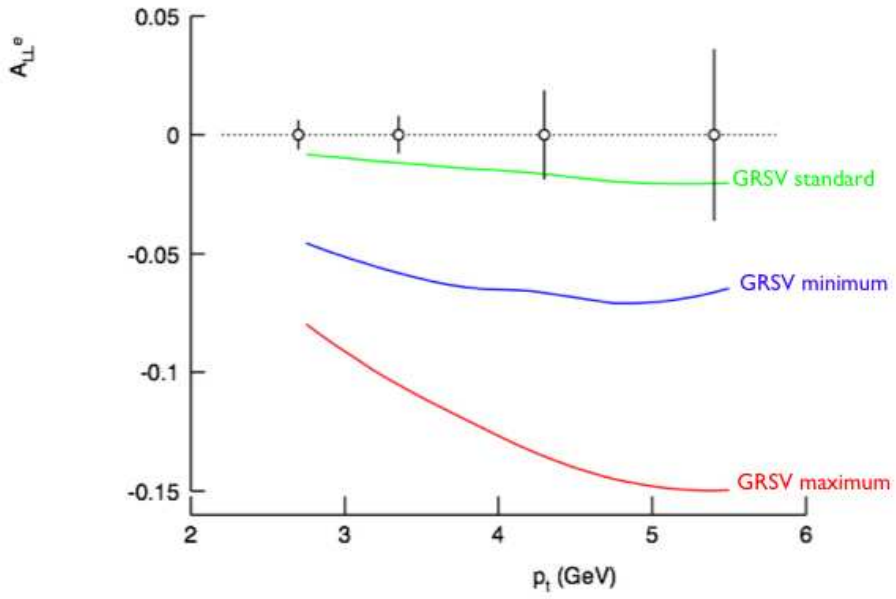

Figure 4: *The longitudinal double-spin asymmetry A_{LL} in $\vec{p}+\vec{p} \to$ charm $\to e + X$ at $\sqrt{s} = 200\,\mathrm{GeV}$ versus electron p_T. The curves show leading order evaluations based on deep-inelastic scattering parametrizations of gluon polarization. The points represent statistical uncertainties for an integrated luminosity of $\sim$100 pb^{-1}, beam polarizations of 70%, and sampling of a 60 cm rms beam-diamond with an inner vertex detector of 20 cm length.*

3 Conceptual layout

3.1 Overview

To reach its full physics capabilities the new Heavy Flavour Tracker needs tracks hitting its outer layers to have good pointing resolution. Unfortunately the TPC tracks have a pointing resolution of around 1000 μm and the existing SSD only improves this in the r-ϕ direction because of its mediocre resolution in the z-direction. The SSD layer (at a radius of 23 cm) will be relativily far from the outer layer of the HFT (at a radius of about 7 cm), which is not optimal for the pointing resolution.

Therefore, we propose to construct a new Intermediate Silicon Tracker (IST) which will provide 2 spacepoints with high accuracy in r-ϕ and z. The IST will consist of two concentric layers between the HFT and the SSD, as shown in figure 5. In the next sections the requirements and the proposed configuration will be discussed.

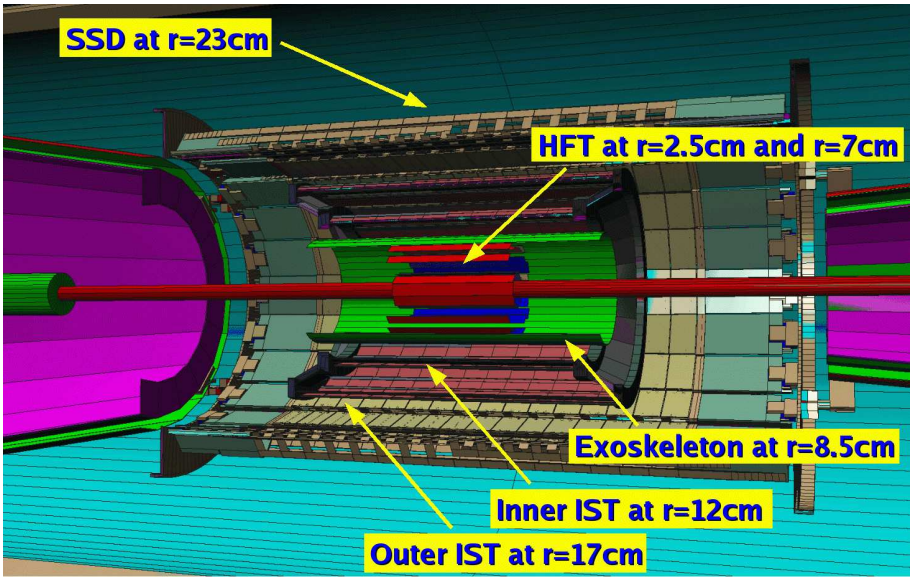

Figure 5: *Side view of the proposed tracking upgrade geometry.*

3.2 Requirements

Radii: The location of the IST layers is constrained by the outer radius of the

Heavy Flavor Tracker (HFT) and the inner radius of the STAR Silicon Strip Detector (SSD). The HFT will occupy space out to a radius of approximately 90 mm and the SSD occupies space into a radius of approximately 190 mm. The most probable radii for the IST layers falls in the range from 90 to 180 mm.

Length: Tracking with the IST is intended to cover the pseudo-rapidity region of $-1 < \eta < 1$ with full coverage of the HFT and fair sampling of the vertex-distribution in STAR. At probable radii between 90 and 170 mm this implies active lengths of 280 to 520 mm.

Multiplicity: If the first layer of the IST is located at a radius of 120 mm then it will be subject to a particle fluence of approximately 1 particle per square centimeter per central Au+Au at 200 GeV. This first layer should be capable of resolving these hits and, as a general rule of thumb, it is desirable to keep the occupancy below 10% .

Mass: The mass requirements for the IST are defined by the heavy ion physics requirements in the mid-rapidity region and by the $W-$boson spin physics program for more forward rapidities. The heavy ion vector meson program, going to di-electrons, is marginal given the existing mass of the SVT in the mid-rapidity region. Similarly, the upsilon program is marginal with the existing mass of the SVT. The IST should thus strive to be as thin or thinner than the current azimuthally averaged 4.5% radiation lenghts of the SVT. The $W-$physics spin program is hindered by SVT support structures in the pseudo-rapidity region of $1 < \eta < 2$. Support structures for the IST should thus be designed to reduce mass in this region.

Thickness per layer: 1% to 1.5% radiation lengths per layer of Si has been routinely achieved by RHIC detectors. The STAR SVT is 1.5% radiation lengths thick per layer and the SSD is 1% radiation length thick when averaged over the full azimuthal range. A new tracker should strive to achieve a comparable or smaller thickness.

Pointing Accuracy: About 18 events will be piled up in the HFT with a 200 μs readout time at the anticipated RHICII luminosity of $90 \cdot 10^{26}\text{cm}^{-2}\text{s}^{-1}$ for Au+Au at 200 GeV. To keep the ghosting level below 5% a pointing resolution to the outer HFT of $170\mu m$ (1σ) is required.

Efficiency and purity The proposed tracking layers should have a tracking efficiency and purity of tracks which is sufficient to do the expected physics programs within a reasonable running time.

Vertex resolution: The vertex resolution of the IST should be adequate to resolve displaced vertices from intermediate to large B-meson decays in

500 GeV p+p collisions.

Intrinsic sampling speed: The spin program at RHIC relies on individual beam bunch crossings to set and determine the relative spin orientations in the proton beams. The IST should be able to resolve individual beam bunches.

Rate capability: The IST should be able to handle the full RHIC-II peak luminosity of $90 \cdot 10^{26}\text{cm}^{-2}\text{s}^{-1}$ for Au+Au at 200 GeV and $4{\cdot}10^{32}\text{cm}^{-2}\text{s}^{-1}$ for p+p.

3.3 Proposed configuration

The Intermediate Silicon Tracker (IST) will consist of two concentric layers, see figure 6. Each layer will be assembled from ladders. Since these ladders, most likely, will have to be glued together, they can be considered as the smallest building block of the IST. There will be two ladder types, their length determined by the layer they will be located in. Each ladder will carry 2 series of silicon sensors arranged back to back. The 'front' and 'back' sensors together will provide 2-dimensional position information. More information about the sensors, mounting structures and readout can be found in section 5. Radii, number of sensors per ladder and number of ladders per layer can be found in table 3.3.

	Layer 1	Layer 2	Total
Radius [mm]	120	170	
No. Sensors per ladder	20	26	
No. Ladders	19	27	
No. Sensors per layer	380	702	1082
No. Readout chips	1900	3510	5410
No. Channels	243200	449280	692480

Table 1: *The characteristics of the IST.*

The current material budget for the two IST layers is shown in figures 7 and 8. The top plots give the observed radiation length versus rapidity and averaged over ϕ. The bottom plots are for the radiation length versus ϕ at mid-rapidity. The minima in the ϕ plots correspond to the radiation length of the two 300 μm silicon sensors in each layer. These results where obtained by propagating 1 million geantinos through the IST geometry using GEANT

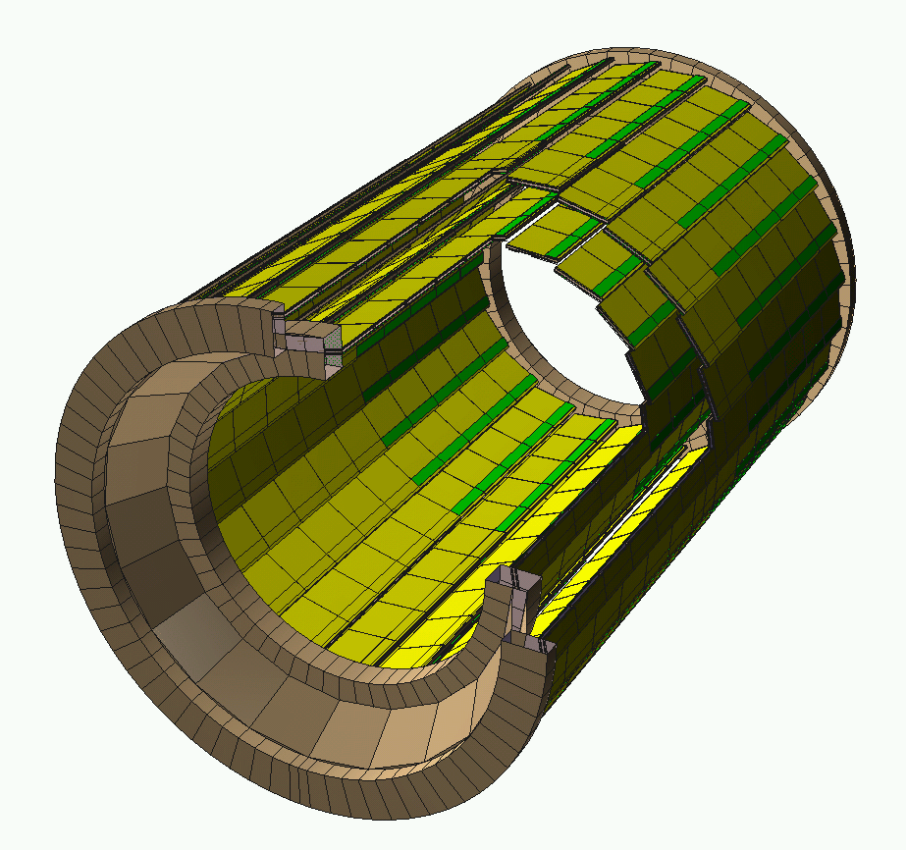

Figure 6: *Geometry drawing of the two IST layers.*

3.21/08. Care was taken to include a realistic estimate for the ladders and cables. The support structures are simplified but should still give an adequate measure of the amount of material.

Figure 9 gives the total material budget for the two layers of the IST. The total material budget for the IST can now be compared with that of the Silicon Vertex Tracker (SVT) shown in figure 10. The IST is doing slightly better than the SVT, although the IST is still under development and care should be taken to keep the material budget at the same level as presented here.

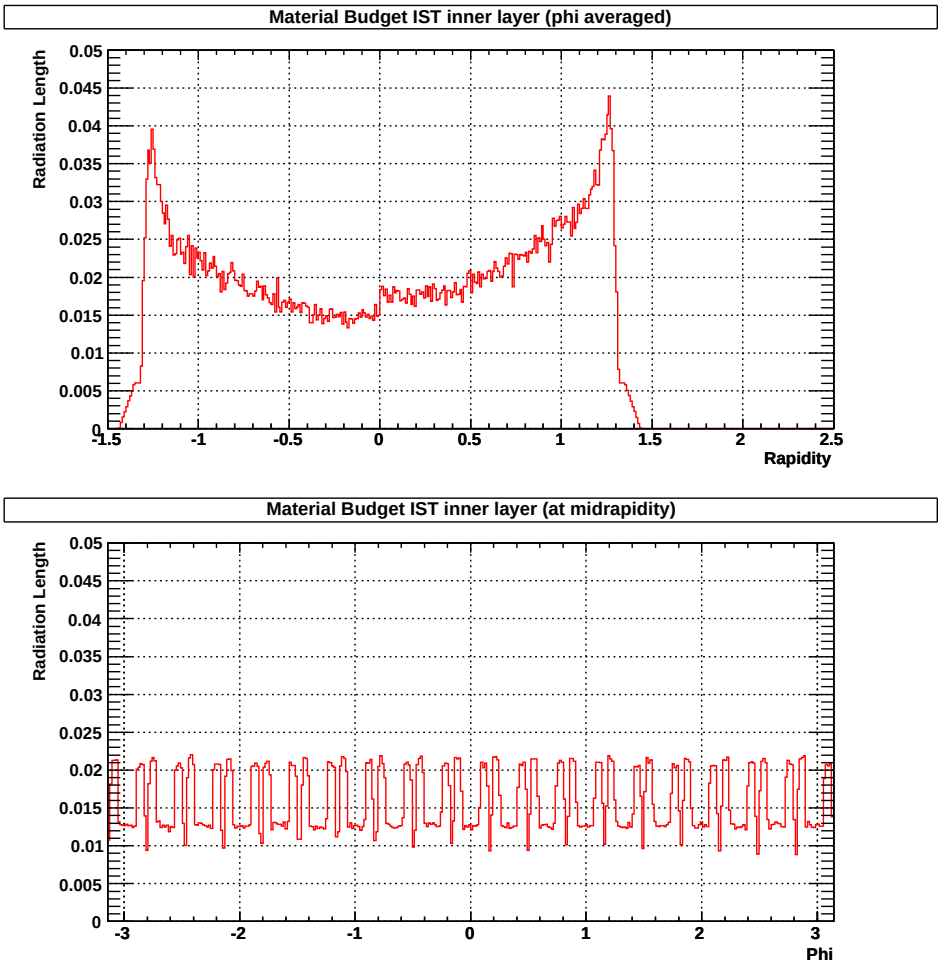

Figure 7: *Material budget versus rapidity (top) and ϕ (bottom) for the inner layer of the IST.*

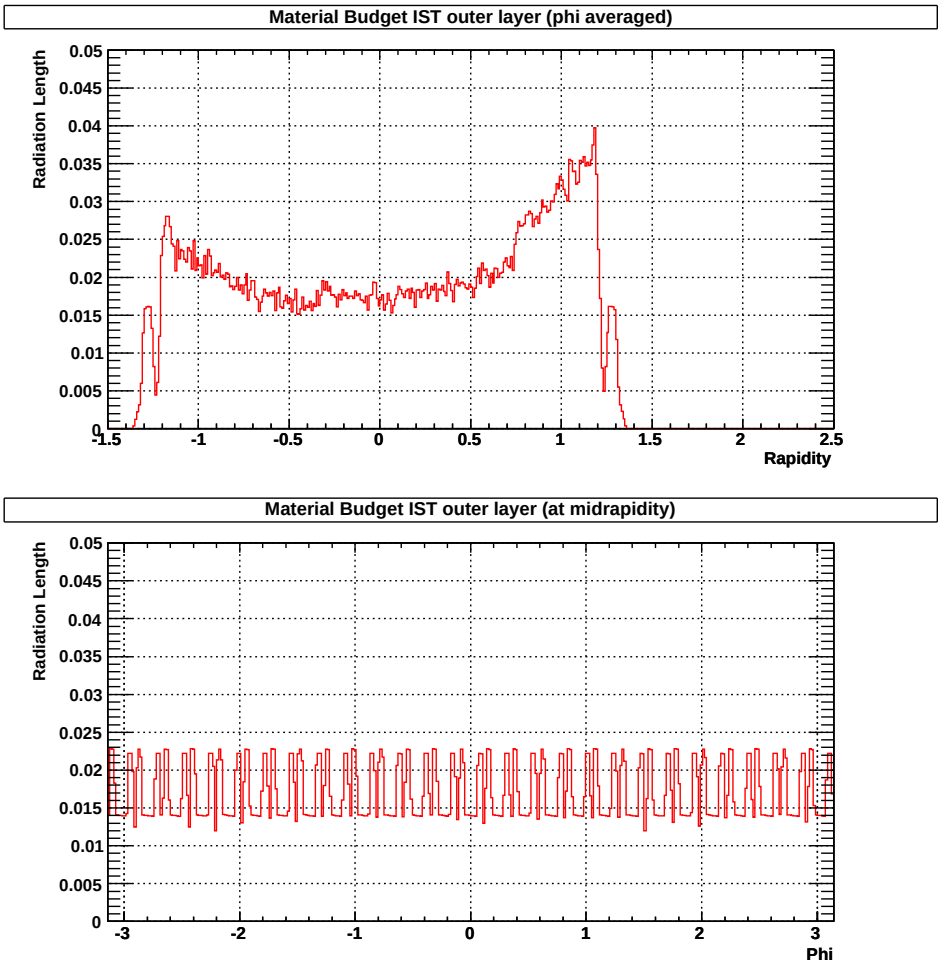

Figure 8: *Material budget versus rapidity (top) and ϕ (bottom) for the outer layer of the IST.*

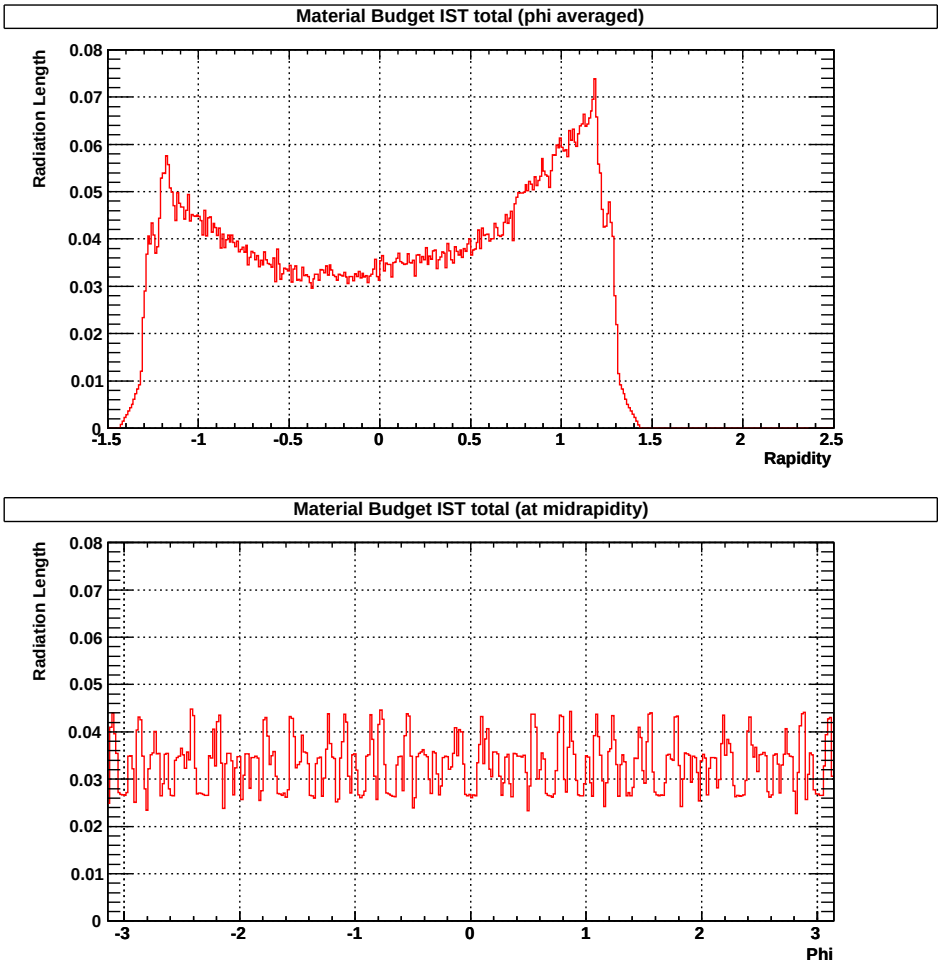

Figure 9: *Total IST material budget versus rapidity (top) and ϕ (bottom).*

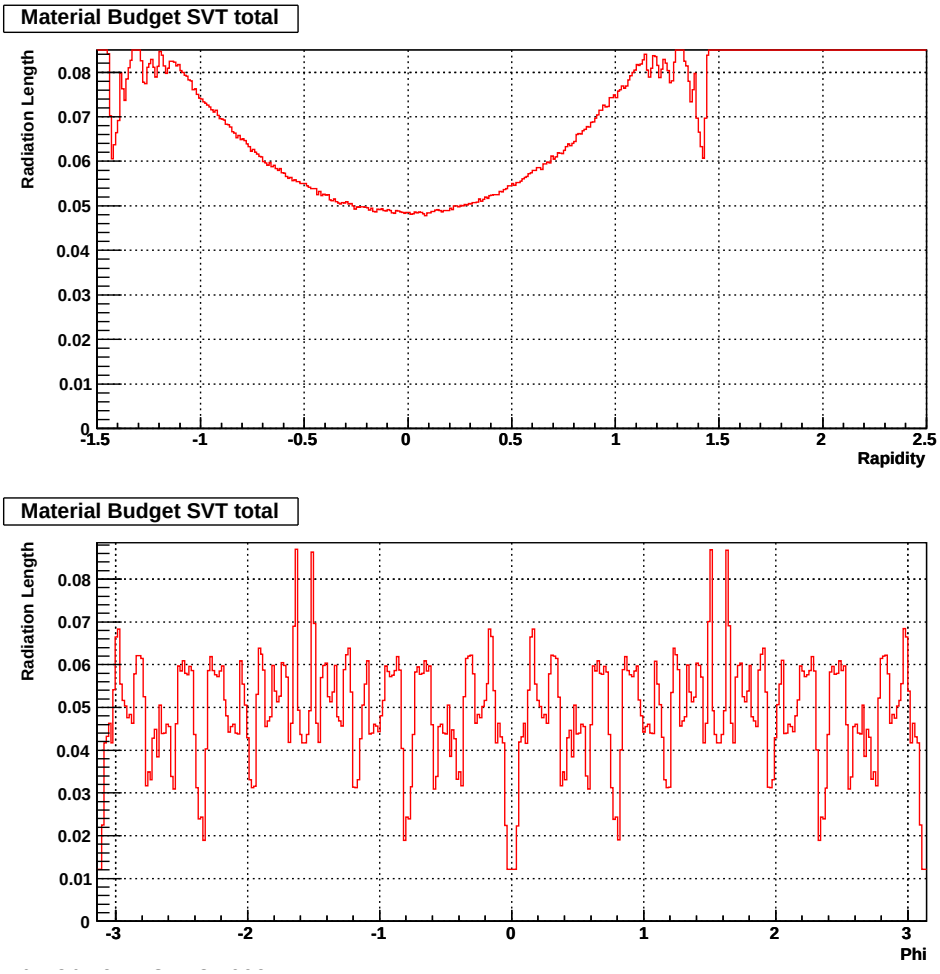

Figure 10: *Total SVT material budget versus rapidity (top) and ϕ (bottom). Note that the y-axis have been forced to the same range as those in figure 9 to facilitate the comparison.*

4 Simulation Results

4.1 Overview

This section describes the current state of the simulation for the inner tracking upgrade. Big progress has been made in all aspects of the simulation framework. HiJing or Pythia events are used to simulate $A+A$ or $p+p$ collisions, respectivily. These events are pushed through GEANT which contains a fairly complete description of the STAR geometry including the tracking upgrade detectors. This stage tracks the primary particles through the geometry, produces secondaries, generates the hits in the detector volumes, but does not digitize the hits. Digitization is supposed to take place in the production phase, but has not been fully implemented yet. This means that detector responses like noise and ambiguous hits can not been studied in a straight-forward way. However, full tracking using the latest STAR tracking software does take place which gives us insight in pointing accuracy, tracking efficiencies, etcetera. Finally, there is a large collection of analysis code which takes the output of the tracking and produces the results and plots presented in this section.

4.2 Occupancy

The high particle densities for central $Au + Au$ collisions at 200GeV pose a big challenge for tracking devices close to the interaction point. The devices be able to keep the occupancies at reasonable levels ($< 10\%$).

Figure 11 shows the particle density as a function of radius. The solid line is just a simple hand calculation taking into account the 700 particles produced in 2π per unit of rapidity at mid-rapidity. The data points are from several different detector configuration and different detectors. The agreement between expectation and simulation is excellent. The figure also shows that at the IST radii of 12 and 17cm the particle density will be around 0.8 and 0.5 particles per cm^2, respectivily. This translates to occupancies of 2% for the inner IST layer and 1% in the outer IST layer. Even when taking a factor of 2 into account for the non-primary particles the occupancies are still tolerable.

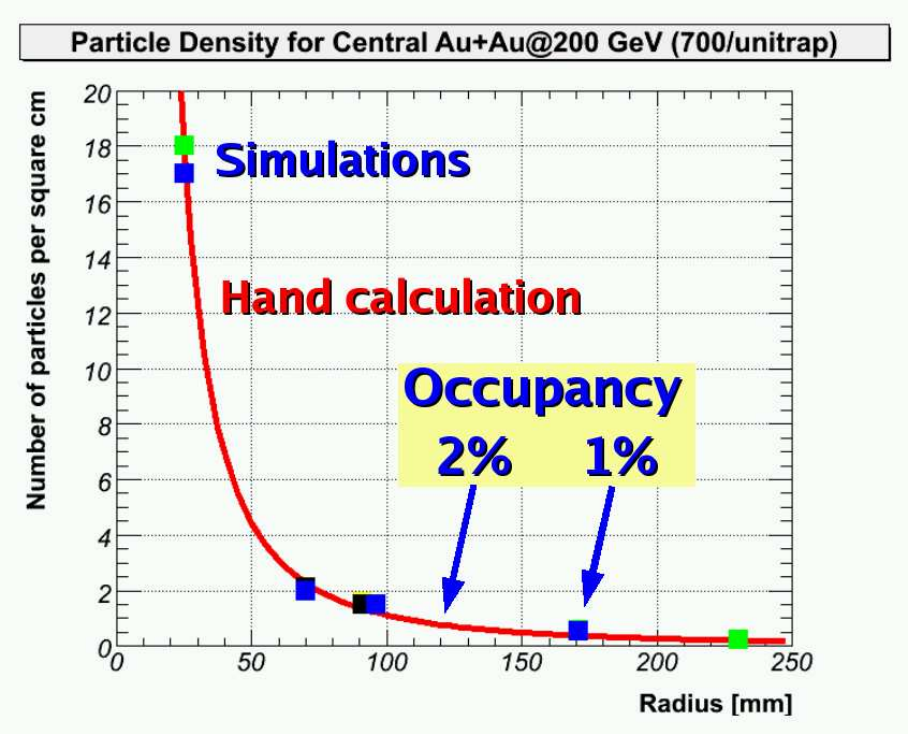

Figure 11: *Particle density at mid-rapidity as a function of radius for central 200 GeV Au + Au collisions. The solid line shows a hand calculation. The data points are obtained from different tracking upgrade detector configurations in a full blown STAR simulation.*

4.3 Pointing to the HFT

An important point of merit is the pointing resolution of the TPC+SSD+IST tracking system on the outer layer of the HFT. This resolution will contribute to resolving hits coming from the event that triggered STAR and the hits coming from pile-up in the HFT. To get a better than 5% ghosting level a pointing resolution of $170\mu m$ (1σ) is required.

Figure 12 shows the $r-\phi$ and z resolution on the outer layer of the HFT for STAR tracking simulations and an advanced hand calculation. The $r-\phi$ resolution is within 1σ while the z resolution is within 3σ. In principle these number could be improved by moving the IST closer to the HFT or by increasing the intrinsic resolution of the IST. The first option comes at the price of higher occupancies and lower tracking efficiencies. The second option

increases the number of channels, power dissipation and overall complexity.

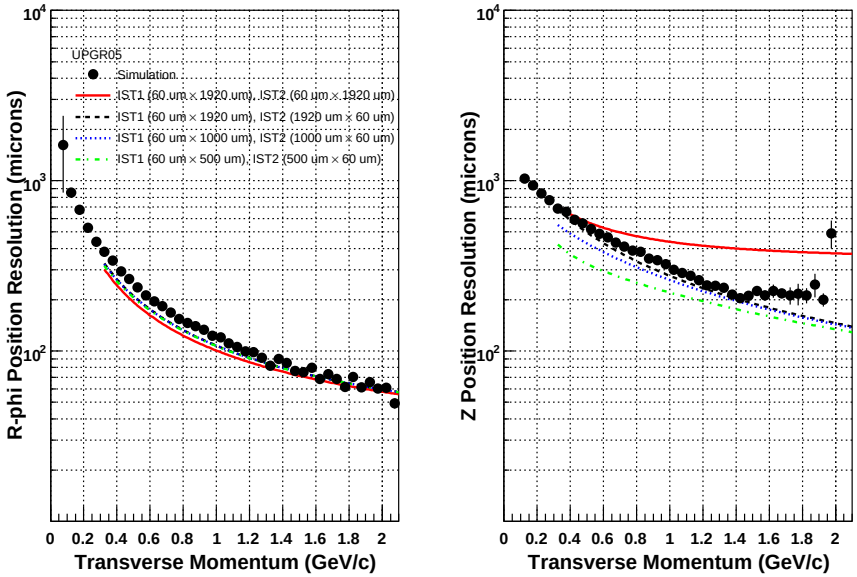

Figure 12: *Pointing resolution in r-ϕ (left) and z (right) for the proposed geometry. The solid circles are determined from the full blown STAR simulations and track reconstruction. The curves are from a hand calculation including tracking and multiple scattering.*

4.4 D0 reconstruction efficiency

In the end what counts is how well $D0$'s can be reconstructed by the new tracking system. There are 2 sets of cuts applied; the tracking cuts and the topological cuts. The tracking cuts select valid tracks by looking for more than 15 TPC hits per track, exactly 2 HFT hits per track and that the track points back to the primary vertex within $50\mu m$. The topological cuts require the $D0$ decay vertex to be more than $50\mu m$ removed from the primary vertex and for the angle between the $D0$ momentum vector and the axis defined by primary and secondary vertex to be less than $200mrad$.

Figures 13 and 14 indicate the power of the TPC+SSD+IST+HFT for finding back primary and secondary vertices. Figure 15 shows how the $D0$

invariant mass spectrum gets cleaned up when applying the the topological cuts. The background, consisting of random combinations between K's and π's, get greatly reduced. This leads to the efficiency of reconstructing a $D0$ shown in figure 16. The efficiency ranges from $\sim$0.6% at a transverse momentum of 1 GeV/c to $\sim$6% at large transverse momenta, demonstrating the feasibility of measurements over a wide kinematic range.

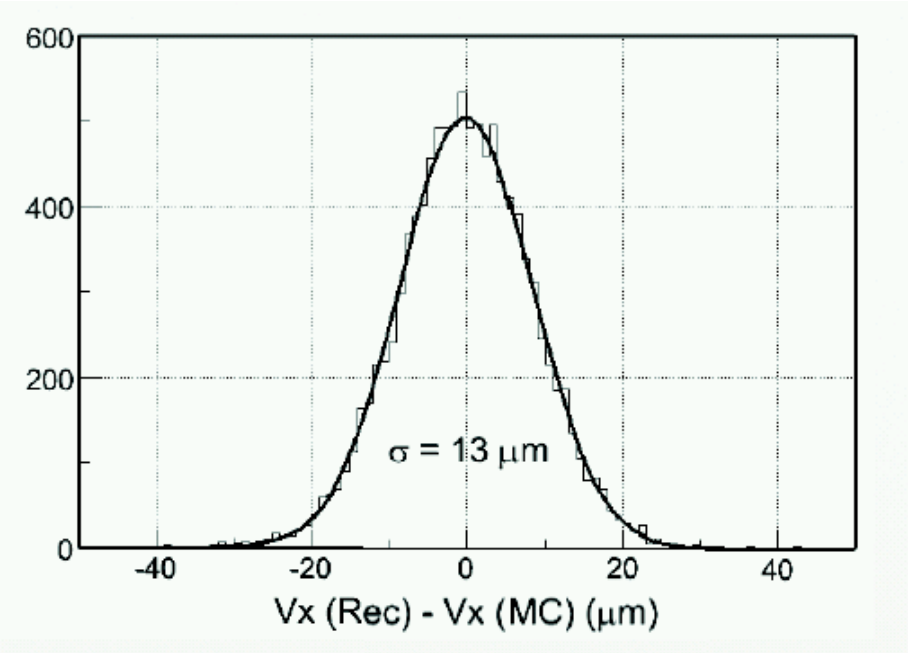

Figure 13: *Resolution of the primary vertex along the z-axis. The resolutions along the y- and z-axis are the same within* $1\mu m$.

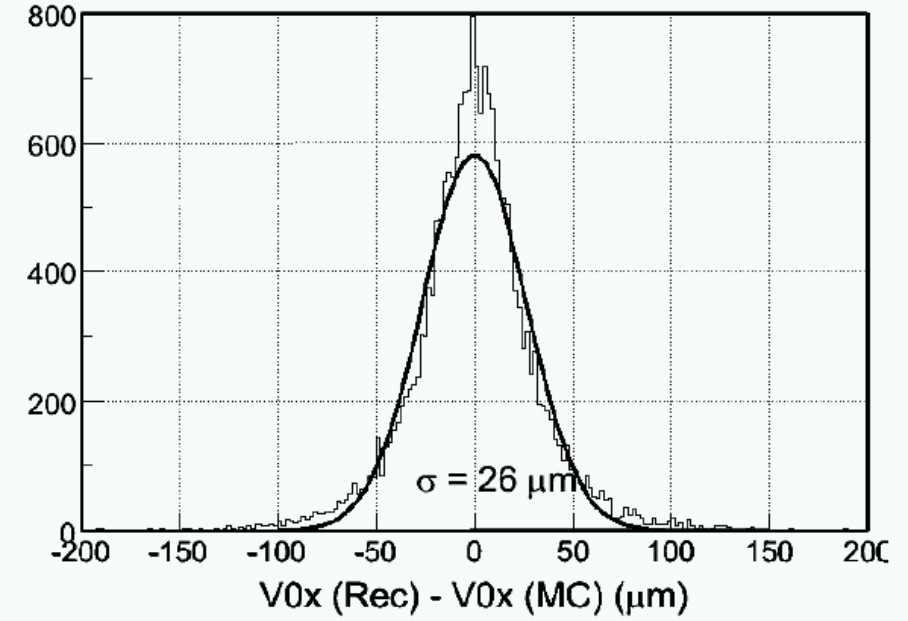

Figure 14: *Resolution of the secondary (D*0 *decay) vertex along the z-axis. The resolutions along the y- and z-axis are the same within* $5\mu m$.

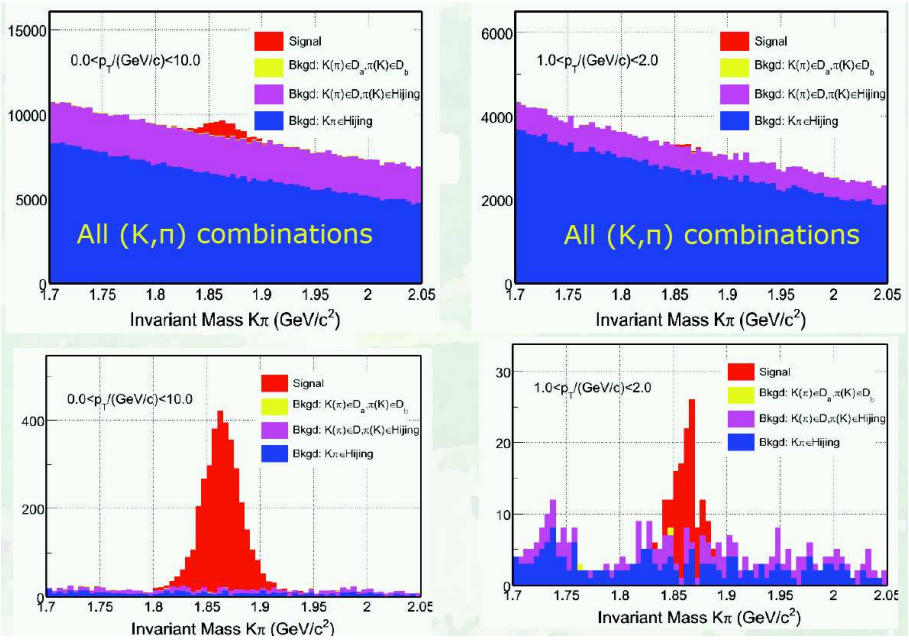

Figure 15: *D0 invariant mass spectrum showing the effect of the applied cuts. The top plots are for tracking cuts only. The bottom plots are with the topological cuts applied.*

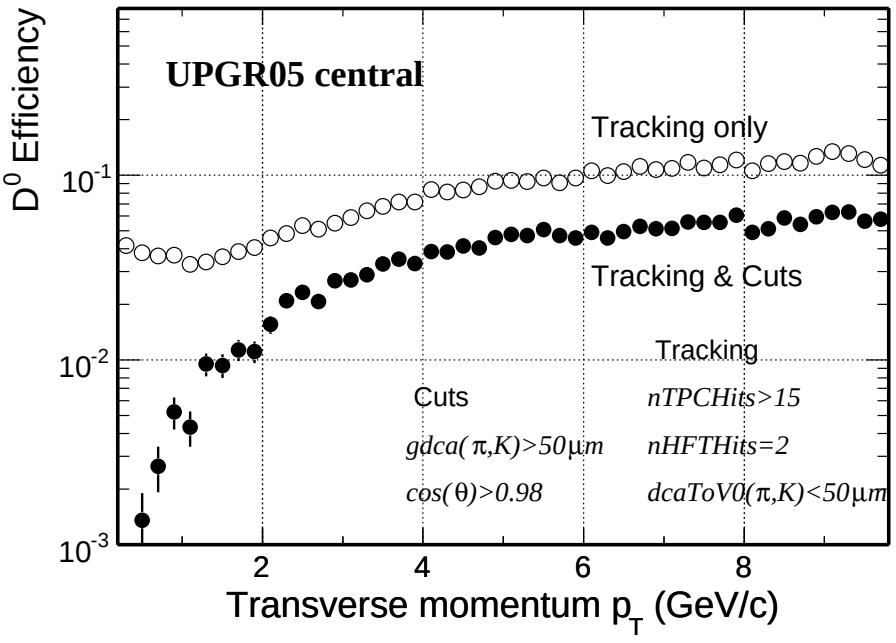

Figure 16: *Efficiency of finding a D0, just from tracking (open circles) and when applying the topological cuts (closed circles).*

5 Technical realization and R&D requirements

5.1 Overview

A combination of well-established silicon strip sensors and silicon pad sensors is foreseen for the IST design. Various technical details will draw to a large extend from previous experience on the design and operation of silicon tracker systems such as the PHOBOS silicon tracker stations. It is foreseen to make use of existing equipment and infrastructure from the PHOBOS silicon tracker through the MIT group.

The following sections will provide an overview of the technical realization of the silicon based tracking systems. The need for R&D will be clearly pointed out where necessary.

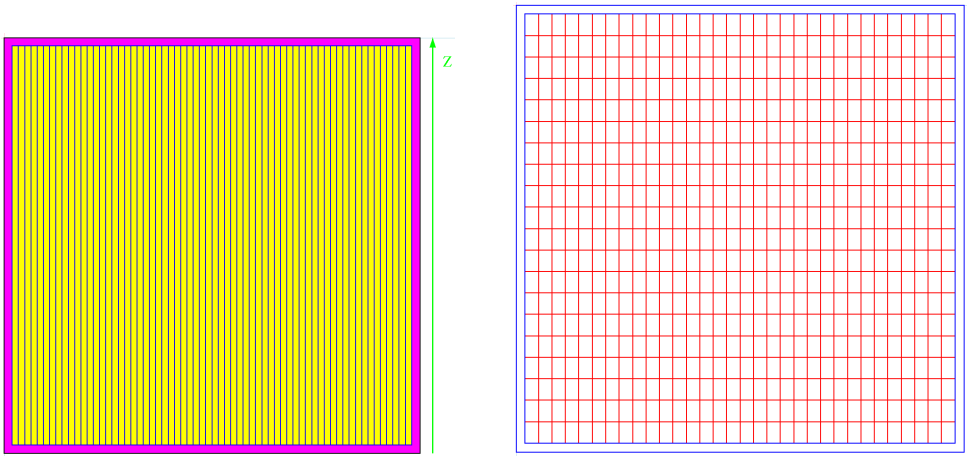

Figure 17: *Sketch of the IST straight (left) and pad (right) sensors.*

5.2 Support structure

The support structure of the intermediate silicon tracker should be both mechanically stable and low mass. The amount of material in this structure will for a large part determine how its performance will be affected by non-desired processes like multiple scattering, conversions, delta rays and nuclear interactions. On the other hand it has to provide a mechanically and thermally stable support for the detector elements. To make it possible to carry out

maintainance work and to accomodate a possible staged installation schedule, the structure also has to be highly modular.

It is foreseen that this support structure will have to support the 2 barrel layers of the intermediate silicon tracker, the 4 disks of the forward silicon tracker and that it will provide a high accuracy mechanical connection for the active pixel detector. It is also possible that it will have to support the existing silicon strip barrel. However, it should be kept in mind that the stiffness, accuracy and final cost of the structure will benefit from keeping its dimensions small.

The mechanical support structure should be made with an overall accuracy of 100μm, which is about the best accuracy which can be achieved for mechanical structures of this size. This overall accuracy will be sufficient to assemble the different parts of the system. Trying to improve on this accuracy would immediately drive up the cost. Locally the structure will have to be more accurate than 100μm. For instance, the mounting surfaces of the sensor modules will have to be flat to within 50μm to avoid stress, and possibly breakage, of the sensors.

The structure should also be thermally sound. It is not foreseen that the detector will be operated other than at room temperature, both during lab testing and while installed in STAR. However, there is always the chance of thermal excursions and the structure should be able to handle those. Preferably the thermal expansion coefficient should be zero. Where this can not be achieved, there should be enough slack to take up the expansion to avoid putting stress on components. For instance, sensor ladders can be mounted only rigidly on one side while the other side is seated in saphire mounts which make longitudinal expansion possible. Also special care should be taken in the choice of adhesives and avoiding 'bimetal' effects during construction of the parts.

A structure made out of carbon fiber composites currently seems the most promising choice. Many groups are using this material to build highly accurate trackers. There is substantial experience, e.g. among the LHC experiments, that we can rely on when designing and building such a complex structure. It is clear that significant R&D is necessary to achieve a low mass system.

5.3 Silicon sensors

The most conservative choice for a silicon tracker is to use silicon strip sensors. The manufacturing techniques for these type of sensors are well established and are mastered by several manufacturers. Silicon strips have been and remain the first choice for most high energy experiment trackers.

The preference is to produce single sided devices with p^+ implants on n-bulk silicon and polysilicon biased. They are relativily easy to produce with high yields and can also be handled without much difficulty in a standard semi-conductor lab. In contrast, double-sided devices have lower yields (so more expensive) and need special equipment to handle them.

To achieve sufficient resolution in two directions with single sided silicon strip sensors it is neccesary to use a stereo pair. This is accomplished by mounting two silicon strip sensors closely back-to-back with one of them having its strips at a certain angle with respect to the other sensor. Unfortunately this option doesn't work well for central Au+Au at 200 GeV/c in the mid-rapidity region. Particle densities of around 1 per cm^2 lead to about 16 particles hitting each envisioned 4 x 4 cm^2 sensor in the first layer of the IST. This leads to unacceptable high numbers of ambiguous hits (ghosts), even when going to very shallow stereo angles with the resolution along the strips going to a few mm.

The proposal is to use back-to-back pairs of silicon strip and silicon pad sensors. The pad sensors would have the same size as the strip sensors (4 x 4 cm^2) but would carry a matrix of about 640 pads. Both the strip sensors and the pad sensors will have a maximum occupancy of about 5%. The rough position of the hit will be given by the pad being hit. Matching with a hit in the strip sensor will improve the resolution in one direction to the strip pitch or better. Ambiguities are much less of an issue than with the stereo strip configuration and are determined by how many strips are covered by a 'column' of pads. The NA34 experiment at the CERN SPS used a similar layout for their silicon telescope to overcome the high particle densities resulting from fixed target kinematics. More recently PHOBOS deployed silicon pad sensors for their spectrometer arms and multiplicity arrays. It is interesting to note that the first layers of the PHOBOS spectrometer arms are very similar to what is proposed here with roughly the same distance from the interaction point.

In total there will be 2 different sensor designs. Figure 17 shows the basics 2 designs for the strip-pad pair in the intermediate silicon tracker (IST).

From the manufacturing point of view all the designs under investigation are reasonably standard.

Preliminary discussions with Hamamatsu have been started about the stereo silicon strip sensor pairs. They are able to make all the designs as we have proposed to them within the budget as described in section 5. We will need to contact them again to inquire after the price and feasibility of the proposed silicon pad sensors.

Table 5.3 provides some information about the sensors that are needed.

	IST strip	IST pad
Number of sensors	618	618
Die size [mm^2]	40 x 40	40 x 40
Number of channels	640	640

Table 2: *The characteristics of the silicon sensors needed for the IST.*

5.4 Ladders and cooling system

A substantial amount of R&D will have to go in developing a low mass and stable ladder structure on which the silicon sensors can be mounted. The best candidate for the ladder material seems to be a thermally conductive carbon foam developed by Oak Ridge National Laboratory. It combines a very low density to high strength and a thermal conductivity close to that of Aluminum.

The inner tracking system will dissipate about 1.5 Watt per sensor assuming 5 APV25-S2 readout chips per sensor. Since the radiation levels are not an issue the system can be kept at room temperature, this avoids problems with condensation and makes maintainance of the system much less complicated.

The current R&D focusses on using air cooling channels through a ladder made out of the thermally conductive carbon foam. By internally shaping the cooling channels an increased turbulence will make the cooling more efficient than just blowing air over the sensors.

5.5 Dry air system

We propose to copy the PHOBOS dry air system which has kept the PHOBOS silicon system at about 10% relative humidity for the duration of the PHOBOS operation. This is a very simple system which boils off liquid nitrogen from a supply tank and feeds it into the almost airtight enclosure of the PHOBOS silicon system. The flow is just enough to maintain a slight overpressure in the enclosure to keep the higher humidity air from the experimental area out of the system. The pressure is regulated by one valve which provides just enough nitrogen boil off to maintain the required overpressure. The system has proven to be very reliable.

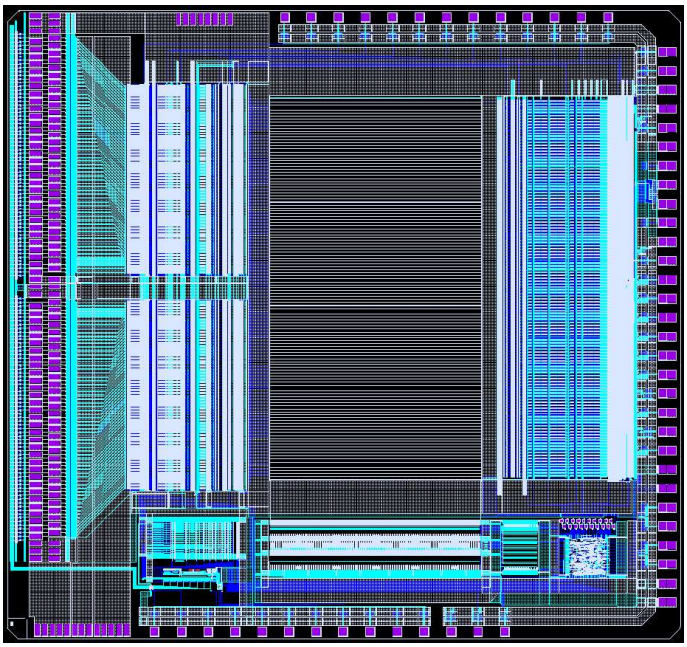

Figure 18: *Picture of the APV25-S1 die. On the left are the input pads, on the right the output pads, control pads, etcetera are visible. The whole die measures 8055 by 7100* μm^2.

5.6 Front-end electronics and DAQ system

The current best estimate is that there will be about 700000 channels to be read out in the IST. Designing and producing specialized readout chips for

this system is not feasible because of the lack of time and manpower. For the sake of expedience it was decided to try to find a readout chip which was already being used for similar purposes by other experiments.

The best candidate so far is the APV25-S1 readout chip which was designed for the CMS silicon tracker and of which about 75,000 will be used in CMS. Each channel of the APV25-S1 chip consists of a charge sensitive amplifier whose output signal is sampled at 40MHz which accounts for the LHC interaction rate. The samples are stored in a $4\mu s$ deep analogue pipeline. Following a trigger the data in the pipeline can be processed by an analoque circuit, mainly deconvoluting the amplifier response from the actual signal and associating the signal with a certain interaction (or rather beam crossing at LHC). The resulting analogue data can then be multiplexed and send to digitizer boards. Although the analogue data leads to higher data volumes at the front-end, it is an enormous advantage that charge sharing between strips and common mode noise can be studied in detail, which will greatly improve the understanding and performance of the detector. The Equivalent Noise Charge (ENC) of the APV25-S1 depends on the capacitance of the strips and the deconvolution algorithm used, but, for our purposes, it will be better than 2000 electrons. With $300\mu m$ thick silicon sensors this will give a signal-to-noise ratio of better than 11:1 when we take the most probably energy deposition by a Minimum Ionizing Particle (MIP). The power consumption of the APV25-S1 is about 2 mW/channel, i.e. about 0.25 Watt/chip. The chips are fabricated in the radiation hard deep sub-micron ($0.25\mu m$) process. Figure 18 shows a closeup of the APV25-S1 chip.

A prototype readout system for the APV25-S1 chips has been designed and is currently being tested. This is part of the triple-GEM prototype effort. The CMS readout system based on optical links is shown in Figure 19.

The STAR radiation environment will be less harsh than that of CMS, it could well be that the front-end digitizers can be located much closer to the detector and that there is no need for 100 meter long analogue optical links. The preference is that the readout system of the silicon system will be the same as for of the GEM system, which is also utilizing the APV25-S1 readout chip. Considering that about 900,000 analogue channels need to be digitized calls for a zero suppresion system as part of the readout system.

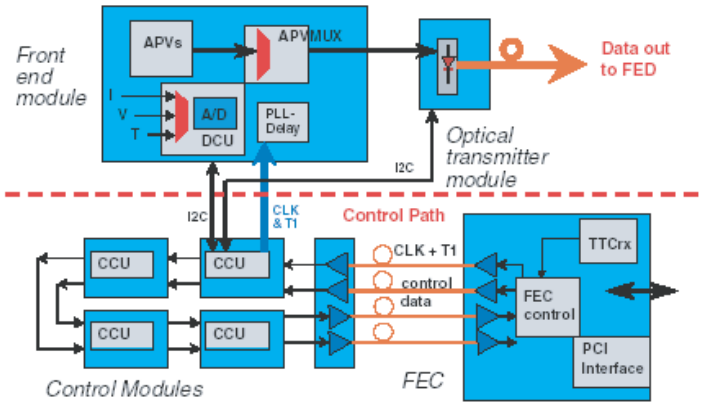

Figure 19: *Block diagram of the APV25-S1 readout system used by CMS.*

5.7 Flex cable/hybrid

To keep the material budget as low as possible a new kapton cable/hybrid cable is under investigation. This flexible cable combines the hybrid, which carries the readout chips, with the long readout cable. This cable will be made out of kapton with a total thickness of about 100μm. The hybrid end will be glued down on the sensor, the other plugs into the a readout unit which will be located just outside of the central TPC area.

Figure 20 shows one of the prototype cables which are currently being usedd for building an IST prototype module.

5.8 High-voltage and low-voltage system

Considering the standard requirements both for the high voltage and low voltage system, those can likely be obtained as almost off the shelf components. Since these systems will be located relativily close to the detector there is the need for remote control and monitoring. Companies like Wiener can build these systems to the desired specifications, including a CANBUS interface.

5.9 Alignment system

The final aligment of the inner silicon tracker will have to be done by tracks. Usually this is done through an itterative residual method. For this method

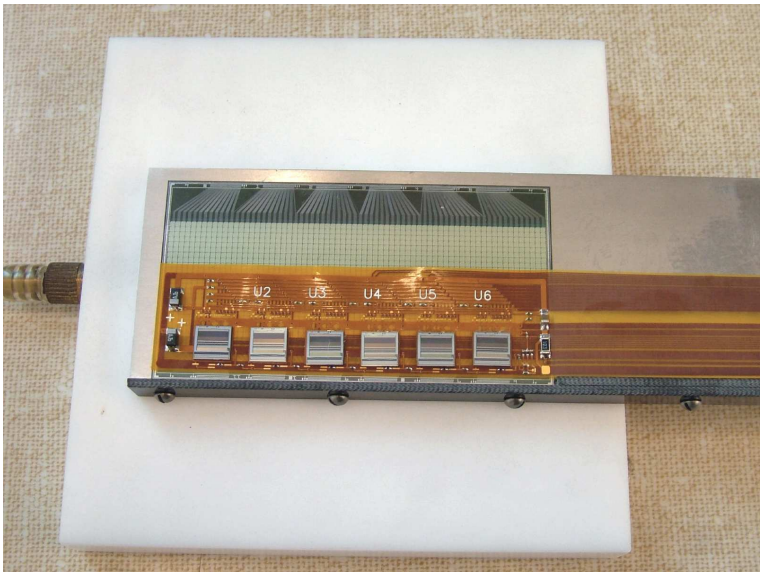

Figure 20: *Prototype cable/hybrid, equiped with readout chips and mounted on a Type 1 PHOBOS silicon pad sensor.*

to work the positions of the strips will have to be known with an accuracy comparable to their width, i.e. $60\mu m$, which is going to be very challenging.

Finding the position of each detector element on a ladder is relativily straightforward. An optical surveying system, which is available at MIT, makes it possible to do this with an accuracy of about $10\,\mu m$ in the plane of the sensors and about $50\,\mu m$ to $100\,\mu m$ perpendicular to the plane of the sensors.

While the ladders are being assembled into barrel layers the next survey step has to be taken. It is very unlikely that the MIT optical surveying station will be able to handle the size of the assembled barrel layers. Logistically it is preferable that the barrel assembly takes place at BNL to avoid shipping of these vulnerable structures from another place to BNL. A touch probe surveying station needs to be found at BNL. Such a system should be able to determine the ladder positions within the inner barrel structure with an accuracy of $50\mu m$ or better. The assembly will then have to take place in 3 stages. First the inner most layer will have to be put together and then surveyed. Then the same needs to be done for the second and then the third layer.

The whole structure has to be stiff enough to retain the surveyed posi-

tions after installation in the STAR magnet. A system with very accurate positioning pins and surfaces will be needed to position the whole system with respect to the Heavy Flavor Tracker.

5.10 Slow control systems

A slow control system has to measure all working parameters of the intermediate and forward silicon tracker. The temperature of the hybrids and the currents and voltages of the components on the hybrids need to be monitored continuously. Also cooling water temperatures, water flow rates and dry air flow rates need to be recorded regulary. Preferably all these monitoring values get enetered into a database. In case that the parameters get out of predefined operating values alarms should be send to the shift crew.

Although STAR is using EPICS as its standard slow control system there is a slight preference to use LabView instead. Labview provides the user with virtually any instrument driver and a very convenient user interface. LabView runs on both Windows and Linux. It is relativily simple to interface LabView and EPICS. However, at the moment, both options are still open.

5.11 Installation procedures

It is foreseen to assemble the complete inner tracking system including a new beam pipe outside, e.g. in the STAR experimental hall. This should include a system test using a cosmic ray test setup. This would also allow to test the integration into the STAR DAQ system at the same time. This step has been proven by many experiments as a critical step for a successful operation after installation. Afer completion of a complete system test, the inner tracking system including a new beam pipe would be then installed as one unit inside STAR.

5.12 Readout system

The APV25S1 Front-End Chip Designing and producing a specialized readout chip for the forward tracking system is not feasible because of manpower and budget constraints. Instead a readout chip that provides the necessary functionality and was developed for another experiment will be used. The best candidate so far is the APV25-S1 readout chip which was designed for the CMS silicon tracker and of which about 75,000 will be used in CMS.

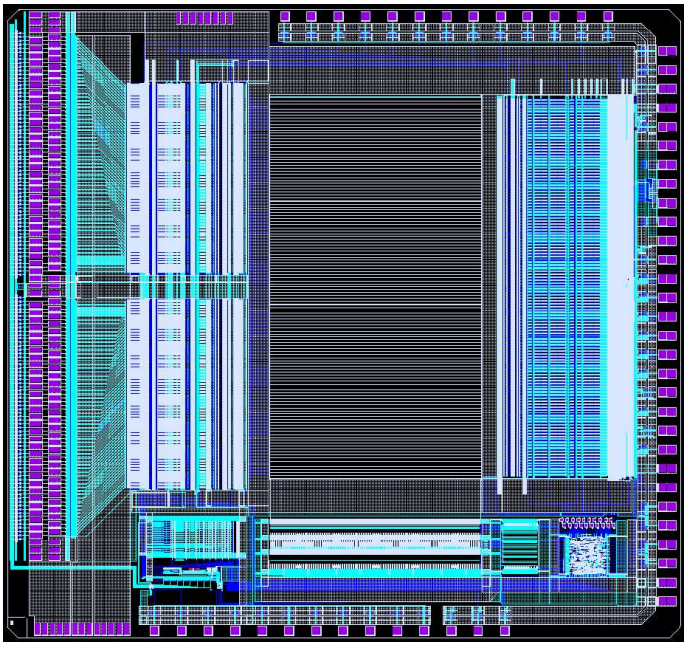

Figure 21: *Picture of the APV25-S1 die. On the left are the input pads, on the right the output pads, control pads, etcetera are visible. The whole die measures 8055 by 7100* μm^2.

An older version of that chip, the AP25-S0 is successfully used with GEM detectors in the COMPASS experiment. Each channel of the APV25-S1 chip consists of a charge sensitive amplifier whose output signal is sampled at 40MHz which accounts for the LHC interaction rate. The samples are stored in a $4\mu s$ deep analogue pipeline. Following a trigger the data in the pipeline can be processed by an analoque circuit, mainly deconvoluting the amplifier response from the actual signal and associating the signal with a certain interaction (or rather beam crossing at LHC). The resulting analogue data can then be multiplexed and send to digitizer boards. Although the analogue data leads to higher data volumes at the front-end, it is an enormous advantage that charge sharing between strips and common mode noise can be studied in detail, which will greatly improve the understanding and performance of the detector. The power consumption of the APV25-S1 is about 2 mW/channel, i.e. about 0.25 Watt/chip. The chips are fabricated in the radiation hard deep sub-micron ($0.25\mu m$) process. Figure 21 shows a closeup of the APV25-S1 chip.

Readout and DAQ Integration Data from the 2D triple-GEM detectors are read out by the APV25-S1 readout system which consists of the following components:

- Signal Boards
- APV Module
- GEM Control Unit

The signal board collects the charge from the detector on a two dimensional strip pattern connected. The boards are fabricated from FR4 as a regular double sided 62mil PC (Printed Circuits) board which has a 50 μm thick Kapton foil glued on top which in turn is covered by 5μm thick and 508 μm wide sensor strips on the bottom and 5μm thick and 127 μm wide sensor strips on the top side in the case of the prototype detectors. Kapton material between top strips is removed through laser etching to uncover the bottom strips which are then gold plated. Signal strips have a 635 μm pitch. The top strips are perpendicular to the bottom strips to form a two dimensional readout board. Each signal strip is connected to the bottom side of the signal board through vias connections and to 635 μm pitch SAMTEC connectors. Those provide then the connections to the APV module. There are two sets of SAMTEC connectors, one for the X and one for the Y direction. The signal board also has two sets of an integrated bus system as part of the communication and data collection between the APV module and GEM control unit.

The GEM Control Unit is the main control system for the 2D GEM readout electronics which controls all ADC, FIFO, and Data formatting and keeps communication between APV25 Modules and DAQ system. A Xilinx CPLD is the heart of each GEM Control Unit. This Xilinx component is fabricated in very deep submicron process (0.095 micron). In radiation tests which were carried out at Bates Linear Accelerator Laboratory, it was found that radiation hardness of the Xilinx CPLD component is beyond 1MRad. The advantage of the Xilinx CPLD is based on the flexibility in re-programming to any desired configuration. Each GEM Control Unit contains for each APV25-S1 an ADC and a FIFO, where the ADC is contiuously running and converting incoming signals from the APV25-S1. Upon a postive trigger decision, the data are then converted and written in parallel into all FIFOs and then in sequence from FIFO by FIFO these data are sent out in LVDS

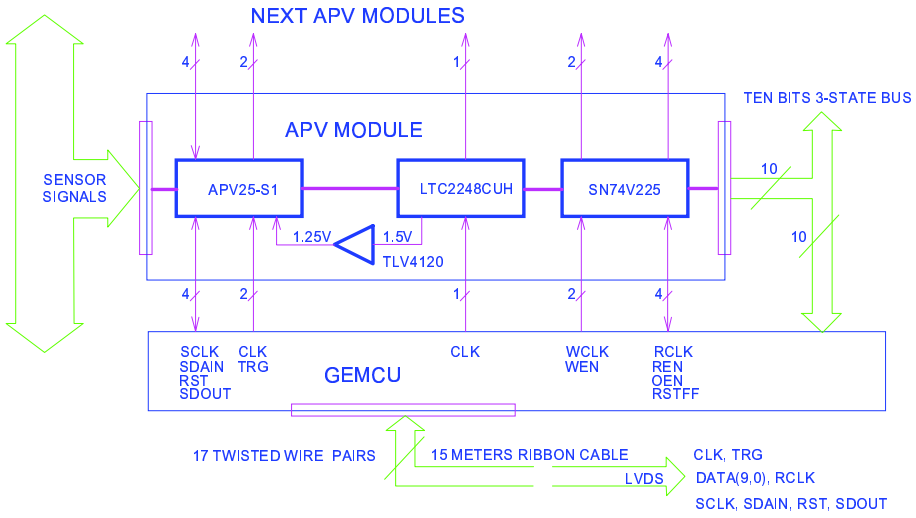

Figure 22: *Sketch of the APV25 chip readout system and STAR DAQ integration.*

standard to the STAR DAQ system. These actions are controlled by the Xilinx CPLD device which is programmed in VHDL language. The GEM Control Unit is connected with the outside environment only through one twenty wire pairs flat ribbon cable. Each GEM Control Unit has all required voltage regulators on board. The power distribution requires therefore only one +4V power supply using one wire pair. Figure 22 shows a sketch of the APV25-S1 chip readout sytem and the STAR DAQ integration.

The signal board, APV25 module and GEM control unit form one compact unit without cables and wires. All connections are realized through PC board printed layer connections. This guarantees that this system will have very low noise.

The full system including STAR DAQ modules was successfully tested with a small resistive plate chamber with cosmic muons. Figure 23 shows one of the events recorded with that setup. The signals in the RPC are much wider than they will be in GEM detectors since the signal pick-up is inductive compared to direct electron collection in a triple GEM device. RPC signals are also much higher, apparent from the fact that most channels reach saturation. While a the charge of a RPC signal is typically between 0.2 pC and 2 pC, a MIP signal in a triple GEM detector is around 10 fC.

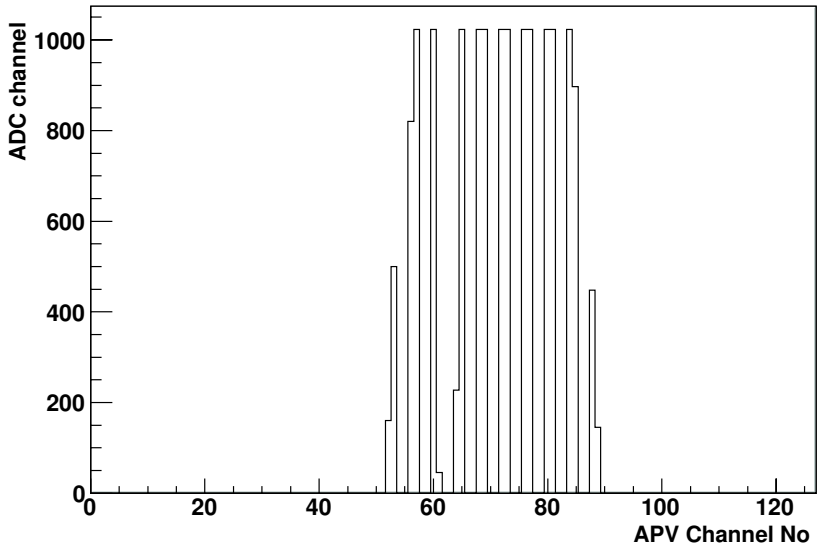

Figure 23: *Cosmic muon pulse in a small RPC recorded with the APV25S1 chip and the full DAQ chain. The two on – two off structure is due to the connection scheme of the APV chip, where only half of the channels are connected to readout strips.*

Nevertheless, these results demonstrate that the full readout chain from the front-end chip to the data acquisition is working as expected.

For tests with a small number of detectors in a low rate environment a USB based readout system for the APV25 and GEM Control Unit is currently being developed. This system allows to install test setups at several locations at low cost, and will be used for GEM detector tests with cosmic muons as well as for beam tests. The DAQ software for this system is based on LabView and can be run on a standard PC or laptop computer.

References

[1] I. Bojak and M. Stratmann, *Phys. Rev.* D67 (2003) 034010.

[2] M. Karliner and R.W. Robinett, *Phys. Lett.* B324 (1994) 209.

[3] *Nuclear Physics A*, Volume 757, Issues 1-2, Pages 1-283 (8 August 2005) First Three Years of Operation of RHIC

[4] D.J. Gross, F. Wilczek, *Phys, Rev. Lett.* 30 (1973) 1343.
H. Politzer, *Phys. Rev. Lett.* 30 (1973) 1346.
Nobel price for physics, 2004.

[5] F. Karsch, *Nucl. Phys. A* 698 (2002) 199.

[6] J.D. Bjorken, FERMILAB-PUB-82-059-T.

[7] M. Gyulassy and M. Plumer, *Phys.Lett.* B243 (1990) 432.

[8] X.N. Wang and M. Gyulassy, *Phys. Rev. Lett.* 68 (1992) 1480.

[9] M. Djordjevic and M. Gyulassy, *Phys. Lett.* B560 (2003) 37.

[10] Anselmino M, Efremov A, Leader E. *Phys. Rep.* 261 (1995) 1; (E) 281 (1997) 399; Cheng HY. *Int. J. Mod. Phys.* A11 (1996) 5109; hep-ph/0002157; Lampe B, Reya E. *Phys. Rep.* 332 (2000) 1; S. Bass, *Eur. Phys. J.* A5 (1999) 17.

[11] Lipkin HJ. *Phys. Lett.* B256 (1991) 284; *Phys. Lett.* B337 (1994) 157; Lichtenstedt J, Lipkin HJ. *Phys. Lett.* B353 (1995) 119.

[12] Adeva B, et al (SMC). *Phys. Lett.* B420 (1998) 180; Ackerstaff K, et al (HERMES Collaboration). *Phys. Lett.* B464 (1999) 123.

[13] Craigie NS, Hidaka K, Jacob M, Renard FM. *Phys. Rep.* 99 (1983) 69; Bourrely C,Soffer J, Leader E. *Phys. Rep.* 59 (1980) 95.

[14] Bourrely C, Soffer J. *Phys. Lett.* B314 (1993) 132; *Nucl. Phys.* B423 (1994) 329; Chiappetta P, Soffer J. *Phys. Lett.* B152 (1985) 126.

[15] Bourrely C, Soffer J. *Nucl. Phys.* B44 (1995) 5341.

[16] Kamal B. *Phys. Rev. D* 57 (1998) 6663.

[17] Gehrmann T. *Nucl. Phys.* B534 (1998) 21.

[18] Bland LC. Presented at Circum-Pan-Pacific RIKEN Symp. High Energy Spin Phys. (Pacific Spin 99), Wako, Jpn., Nov. 1999. hep-ex/0002061 (2000)

[19] Gehrmann T, Stirling WJ. *Phys. Rev. D* 53:((191)996) 6100.

[20] Sjostrand T. *Comput. Phys. Commun.* 82 (1994) 74.

[21] Balazs C, Yuan C.-P. *Phys. Rev. D* 56 (1997) 5558.

[22] Abe F, et al (CDF Collaboration). *Phys. Rev. Lett.* 74 (1995) 850; *Phys. Rev. Lett.* 81 (1998) 5754.

[23] Gottfried K. *Phys. Rev. Lett.* 18 (1967) 1174.

[24] CTEQ Collaboration, Lai HL, et al. *Phys. Rev. D* 55 (1997) 1280.

[25] Martin AD, Roberts RG, Stirling WJ, Thorne RS. *Eur. Phys. J.* C14 (2000) 133.

[26] Vogelsang W. et al. *Phys. Rev.* D63 (2001) 094005.

[27] STAR collaboration, Heavy-Flavor Tracker proposal, Internal document.